PHYSICAL REVIEW B **90**, 020502(R) (2014)

Multiband transport and nonmetallic low-temperature state of $K_{0.50}Na_{0.24}Fe_{1.52}Se_2$

Hyejin Ryu (류혜진),[1,2,*] F. Wolff-Fabris,[3,†] J. B. Warren,[4] M. Uhlarz,[3] J. Wosnitza,[3,5] and C. Petrovic[1,2,‡]

[1]*Condensed Matter Physics and Materials Science Department, Brookhaven National Laboratory, Upton, New York 11973, USA*

[2]*Department of Physics and Astronomy, Stony Brook University, Stony Brook, New York 11794-3800, USA*

[3]*Hochfeld-Magnetlabor Dresden (HLD), Helmholtz-Zentrum Dresden-Rossendorf, D-01314 Dresden, Germany*

[4]*Instrument Division, Brookhaven National Laboratory, Upton, New York 11973, USA*

[5]*Institut für Festkörperphysik, TU Dresden, D-01062, Dresden, Germany*

(Received 6 December 2013; published 8 July 2014)

We report evidence for multiband transport and an insulating low-temperature normal state in superconducting $K_{0.50}Na_{0.24}Fe_{1.52}Se_2$ with $T_c \approx 20$ K. The temperature-dependent upper critical field H_{c2} is well described by a two-band BCS model. The normal-state resistance, accessible at low temperatures only in pulsed magnetic fields, shows an insulating logarithmic temperature dependence as $T \to 0$ after superconductivity is suppressed. This is similar as for high-T_c copper oxides and granular type-I superconductors, suggesting that the superconductor-insulator transition observed in high magnetic fields is related to intrinsic nanoscale phase separation.

DOI: 10.1103/PhysRevB.90.020502 PACS number(s): 74.25.F−, 72.80.Ga, 74.70.Xa, 74.81.−g

After the discovery of $LaFeAsO_{1-x}F_x$ with $T_c = 26$ K [1], many efforts have been made to study the temperature dependence of the upper critical field H_{c2} of Fe-based superconductors since this provides valuable insight in the coherence length, anisotropy, electronic structure, and the pair-breaking mechanism. Binary β-FeSe and Fe_{1+y}(Te,Se) (FeSe-11 type) as well as arsenic-deficient CuZrSiAs structure-type superconductors (FeAs-1111 type) feature a Pauli-limited H_{c2} and are well explained by the single-band Werthamer-Helfand-Hohenberg (WHH) model [2–5]. On the other hand, in most FeAs-1111 type, ternary pnictide (FeAs-122 type), and chalcogenide (FeSe-122 type) Cu_2TlSe_2 Fe-based superconductors, H_{c2} can only be described by two-band models [6–9]. Studies of the normal state below T_c in both Cu- and Fe-based high-T_c superconductors are rare since very high magnetic fields are required to suppress the superconductivity. Among the few exceptions are studies of $La_{2-x}Sr_xCuO_4$ and $Bi_2Sr_{2-x}La_xCuO_6$, where a logarithmic resistivity and a superconductor-insulator transition (SIT) have been observed in the normal-state region above H_{c2} and below T_c [10–12]. Similar studies in FeSe-122-type superconductors have not been available so far due to their air sensitivity and the demanding experimental conditions of pulsed-field experiments.

In this Rapid Communication, we report on results obtained for single-crystalline $K_{0.50}Na_{0.24}Fe_{1.52}Se_2$ with $T_c \approx 20$ K. $H_{c2}(T)$ is well described by a two-band model. Moreover, when superconductivity is suppressed in high magnetic fields, the in-plane sample resistance follows $R_{ab} \propto \ln(T)$ as $T \to 0$, suggesting a SIT, as commonly observed in granular superconductors.

The $K_{0.50(1)}Na_{0.24(4)}Fe_{1.52(3)}Se_{2.00(5)}$ single crystals used in this study were synthesized and characterized as described previously with a nominal composition of starting materials K:Na:Fe:Se = 0.6:0.2:2:2 [13]. The as-grown crystals were sealed in a Pyrex tube under vacuum ($\sim 10^{-1}$ Pa), annealed at 400 °C for 3 h, and then quenched in air in order to increase the superconducting volume fraction [14–16]. Powder x-ray diffraction (XRD) spectra were taken with Cu$K\alpha$ radiation ($\lambda = 0.154\,18$ nm) by a Rigaku Miniflex x-ray machine. The lattice parameters were obtained by refining XRD spectra using the RIETICA software [17]. The elemental analysis was done using a scanning electron microscope (SEM). Magnetization measurements were performed in a Quantum Design magnetic property measurement system (MPMS-XL5). The ac magnetic susceptibility was measured with an excitation frequency of 100 Hz and field of 1 Oe. Electrical-resistivity measurements were conducted using a standard four-probe method in a physical property measurement system (PPMS-14). Pulsed-field experiments were performed up to 62 T using a magnet with 150 ms pulse duration and data were obtained via a fast data acquisition system operating with ac current in the kHz range. Contacts were made on freshly cleaved surfaces inside a glove box.

The powder XRD data [Fig. 1(a)] demonstrate the phase purity of our samples without any extrinsic peak present. The pattern is refined in the space groups $I4/mmm$ and $I4/m$ with fitted lattice parameters $a = 0.3870(2)$ nm, $c = 1.4160(2)$ nm and $a = 0.8833(2)$ nm, $c = 1.4075(2)$ nm, respectively, reflecting phase separation and small sample yield [18–23]. With Na substitution, the lattice parameter a decreases while c increases when compared to $K_{0.8}Fe_2Se_2$, consistent with lattice parameters of $NaFe_2Se_2$ [24,25]. The average stoichiometry was determined by energy-dispersive x-ray spectroscopy (EDX), measuring multiple positions on the crystal. The obtained composition $K_{0.50(1)}Na_{0.24(4)}Fe_{1.52(3)}Se_{2.00(5)}$ suggests vacancies on both K and Fe sites. FeSe-122 superconductors feature an intrinsic phase separation into magnetic insulating and superconducting regions [19–23]. As shown in the SEM image of Fig. 1(b), $K_{0.50(1)}Na_{0.24(4)}Fe_{1.52(3)}Se_2$ also exhibits a similar array of superconducting grains in an insulating matrix. The observed pattern is somewhat inhomogeneous [Fig. 1(b)] with sizes ranging from about several microns to probably several tens of nanometers [20], below our resolution limit. It would be of interest to investigate the local structure

*hryu@bnl.gov

†Present address: European XFEL GmbH, Notkestrasse 85, 22607 Hamburg, Germany.

‡petrovic@bnl.gov

 ©2014 American Physical Society

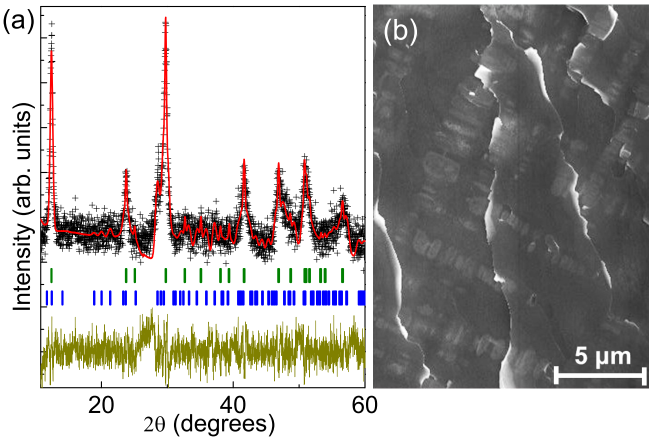

FIG. 1. (Color online) (a) Powder XRD pattern of $K_{0.50(1)}Na_{0.24(4)}Fe_{1.52(3)}Se_2$. The plot shows the observed (+) and calculated (solid red line) powder pattern with the difference curve underneath. Vertical tick marks represent Bragg reflections in the $I4/mmm$ (upper green marks) and $I4/m$ (lower blue marks) space group. (b) SEM image of the crystal.

and electronic properties of $K_{0.50(1)}Na_{0.24(4)}Fe_{1.52(3)}Se_{2.00(5)}$ since Na substitution provides chemically induced pressure which might suppress the phase separation, similar as for $Rb_{1-x}Fe_{2-y}Se_2$ [26].

The investigated single crystal becomes superconducting at 20 K after and at 28 K before the annealing and quenching procedure [Fig. 2(a), the main part and inset, respectively] [14,15].

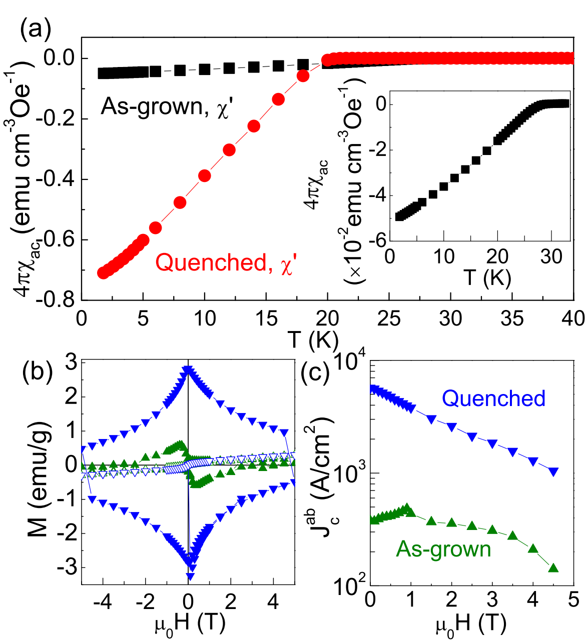

FIG. 2. (Color online) (a) Temperature dependence of the ac magnetic susceptibilities of as-grown (magnified in the inset) and quenched $K_{0.50(1)}Na_{0.24(4)}Fe_{1.52(3)}Se_2$. (b) Magnetic hysteresis loops of as-grown (triangles) and quenched (inverted triangles) samples at $T = 1.8$ K (solid symbols) and $T = 300$ K (open symbols) for $H\|c$. (c) Superconducting critical-current densities $J_c^{ab}(\mu_0 H)$ at $T = 1.8$ K.

For the quenched crystal, the superconducting volume fraction at 1.8 K increases significantly up to 72%, albeit with a reduction of T_c. The postannealing and quenching process results in a surface oxidation of some crystals which then dominates the magnetization signal. However, Fe_3O_4 is not visible in either of our laboratory or synchrotron x-ray studies [14–16]. The magnetic hysteresis loops (MHLs) of the quenched $K_{0.50(1)}Na_{0.24(4)}Fe_{1.52(3)}Se_2$ single crystal reflect the improvement in crystalline homogeneity since it is much larger and symmetric when compared to an as-grown sample [Fig. 2(b)] due to stronger pinning forces and bulk pinning [14]. Also similar to $K_xFe_{2-y}Se_2$, there is an enhancement of the in-plane critical-current density calculated from the Bean model [27,28], $J_c^{ab}(\mu_0 H) = \frac{20\Delta M(\mu_0 H)}{a(1-a/3b)}$, where a, b, and c are the lengths of a rectangularly shaped crystal ($b > a > c$). In view of the improved volume fraction and homogeneity, further investigations of the electronic transport properties were performed on the quenched crystal.

The resistance of an inhomogeneous sample contains contributions from both metallic (R_m) and nonmetallic (R_i) regions. At $T < T_c$, due to superconductivity ($R_m = 0$), the insulating part of the sample is short circuited. The insulating regions have a several orders of magnitude higher resistivity than the metallic part [29]; hence, around T_c and when $T \to 0$ in the high-field normal state, $R(T) \approx R_m(T)$. This is similar to the resistance of a polycrystalline sample in the presence of grain boundaries, and in agreement with the observation that insulating regions do not contribute to the spectral weight in angular resolved photoemission data in the energy range near E_F [30]. In what follows below, we focus on the temperature-dependent sample resistance $R(T)$.

The superconducting transition in $R_{ab}(T)$ is rather wide and shifts to lower temperatures in applied magnetic fields [Figs. 3(a)–3(d)]. The shift is more pronounced for $H\|c$, which implies an anisotropic $\mu_0 H_{c2}$. The temperature-dependent upper critical fields shown in Fig. 3(c) were determined from the resistivity drops to 90%, 50%, and 10% of the normal-state value. It is clear that all experimental data feature a similar temperature dependence irrespective of the criteria used. All data for $H\|c$ are above the expected values for the single-band Werthamer-Helfand-Hohenberg (WHH) model (dotted lines). We proceed our further analysis using the 10% values, similar as done for $LaFeAsO_{0.89}F_{0.11}$ [6]. The $H_{c2}(T)$ curves are linear for $H\perp c$ near T_c and show an upturn at low T for $H\|c$ [Fig. 3(e)]. The initial slope near T_c for $H\perp c$ is much larger than for $H\|c$ [Fig. 3(f) and Table I]. These slopes are similar to values for as-grown and quenched $K_xFe_{2-y}Se_2$ [9,31].

There are two basics mechanisms of Cooper-pair breaking by magnetic field in a superconductor. Orbital pair breaking imposes an orbital limit due to the induced

TABLE I. Superconducting parameters of the quenched $K_{0.50(1)}Na_{0.24(4)}Fe_{1.52(3)}Se_2$ single crystal.

	T_c (K)	$(d\mu_0 H_{c2}/dT)\|_{T=T_c}$ (T/K)	$\mu_0 H_{c2}(0)$ (T)	$\xi(0)$ (nm)
$H\perp c$	14.1(5)	−4.3(3)	150–160	2.62–2.95
$H\|c$	14.1(5)	−1.1(2)	38–48	0.75–0.79

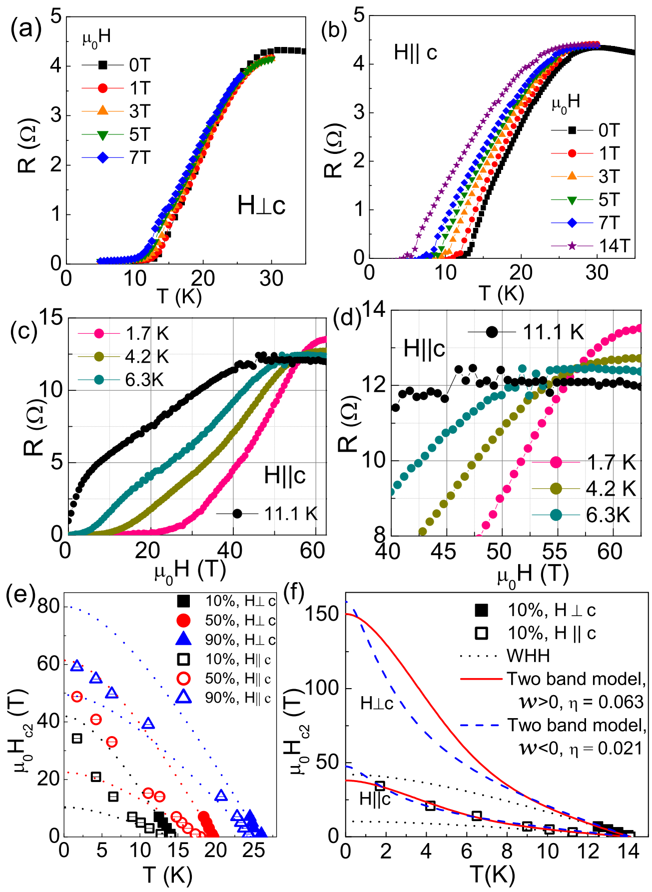

FIG. 3. (Color online) In-plane resistivity of $K_{0.50(1)}Na_{0.24(4)}Fe_{1.52(3)}Se_2$ for (a) $H\perp c$ and (b) $H\|c$. $R_{ab}(T)$ measured at various temperatures in pulsed magnetic fields up to 63 T in the full field range (c) and near the $H_{c2}(T)$. (e) Temperature dependence of the resistive upper critical field $\mu_0 H_{c2}$ determined using three different criteria (10%, 50%, and 90% of the normal-state value). Dotted lines are the WHH plots. (f) Superconducting upper critical fields for $H\perp c$ (solid symbols) and $H\|c$ (open symbols) using Eq. (1) with different pair-breaking mechanisms: (1) WHH (dotted line), (2) two-band model with $w > 0$, $\eta = 0.063$ (solid line), and (3) two-band model with $w < 0$, $\eta = 0.021$ (dashed line).

screening currents, whereas the Zeeman effect contributes to the Pauli paramagnetic limit of H_{c2}. In the single-band WHH approach, the orbital critical field is given by $\mu_0 H_{c2}(0) = -0.693 T_c (d\mu_0 H_{c2}/dT)|_{T=T_c}$ [32]. For $K_{0.50(1)}Na_{0.24(4)}Fe_{1.52(3)}Se_2$, this leads to 42(3) T for $H\perp c$ and 10(2) T for $H\|c$ [Fig. 3(f)]. On the other hand, the Pauli-limiting field is given by $\mu_0 H_p(0) = 1.86 T_c (1 + \lambda_{e\text{-ph}})^{1/2}$, where $\lambda_{e\text{-ph}}$ is the electron-phonon coupling parameter [33]. Assuming $\lambda_{e\text{-ph}} = 0.5$, which is a typical value for a weak-coupling BCS superconductor [34], $\mu_0 H_p(0)$ is 32(1) T. This is larger than the orbital pair-breaking field for $H\|c$ estimated above, yet smaller than the value for $H\perp c$, which possibly implies that electron-phonon coupling is much stronger than for typical weak-coupling BCS superconductors.

The experimental data for $\mu_0 H_{c2}(0)$ lie above the expected values from WHH theory [Fig. 3(f)], suggesting that multiband effects are not negligible. In the dirty limit, the upper critical field found for the two-band BCS model with orbital pair breaking and negligible interband scattering is [35]

$$a_0[\ln t + U(h)][\ln t + U(\eta h)] + a_2[\ln t + U(\eta h)] + a_1[\ln t + U(h)] = 0, \tag{1}$$

$$U(x) = \psi(1/2 + x) - \psi(1/2), \tag{2}$$

where $t = T/T_c$, $\psi(x)$ is the digamma function, $\eta = D_2/D_1$, D_1 and D_2 are diffusivities in band 1 and band 2, $h = H_{c2}D_1/(2\phi_0 T)$, and $\phi_0 = 2.07\times10^{-15}$ Wb is the magnetic flux quantum. $a_0 = 2w/\lambda_0$, $a_1 = 1 + \lambda_-/\lambda_0$, and $a_2 = 1 - \lambda_-/\lambda_0$, where $w = \lambda_{11}\lambda_{22} - \lambda_{12}\lambda_{21}$, $\lambda_0 = (\lambda_-^2 + 4\lambda_{12}\lambda_{21})^{1/2}$, and $\lambda_- = \lambda_{11} - \lambda_{22}$. λ_{11} and λ_{22} are pairing (intraband coupling) constants in band 1 and 2, and λ_{12} and λ_{21} quantify interband couplings between band 1 and 2. For $D_1 = D_2$, Eq. (1) simplifies to the one-band model (WHH) in the dirty limit [32]. When describing our data by use of the two-band BCS model fitting, we consider two different cases, $w > 0$ and $w < 0$, which imply either dominant intraband or dominant interband coupling, respectively. The solid lines in Fig. 3(f) are fits using Eq. (1) for $\lambda_{11} = \lambda_{22} = 0.5$ and $\lambda_{12} = \lambda_{21} = 0.25$, which indicates strong intraband coupling [7,36]. The extrapolated $\mu_0 H_{c2}(0)$ is ~38 T for $H\|c$ and ~150 T for $H\perp c$. Further, the dashed lines in Fig. 3(f) show fits with $\lambda_{11} = \lambda_{22} = 0.49$ and $\lambda_{12} = \lambda_{21} = 0.5$ for strong interband coupling [7,36] that give $\mu_0 H_{c2}(0)$ ~48 T for $H\|c$ and ~160 T for $H\perp c$.

From these fits we obtain η values of 0.063 and 0.021 for dominant intraband ($w > 0$) and interband ($w < 0$) coupling, respectively, i.e., largely different D_1 and D_2 implying different electron mobilities in the two bands. The upward curvature of $\mu_0 H_{c2}(T)$ is governed by η; it is more pronounced for $\eta \ll 1$. The large difference in the intraband diffusivities could be due to pronounced differences in effective masses, scattering, or strong magnetic excitations [7,35]. The fit results are not very sensitive to the choice of the coupling constants, yet they mostly depend on η. This indicates either similar interband and intraband coupling strengths or that their difference is beyond our resolution limit. Our results are consistent with the data obtained on pure crystals, i.e., the large difference of electronic diffusivities for different Fermi surface sheets is maintained in the doped crystal [37]. This is in agreement with the band-structure calculations that showed a negligible contribution of K to the Fermi surface and density of states at the Fermi level [38,39]. On the other hand, we find no enhancement of the superconducting T_c with Na substitution in $K_xFe_{2-y}Se_2$ ($T_c \sim 30$ K). This is somewhat surprising because $Na_xFe_2Se_2$ and $NaFe_2Se_2$ that crystallize in the $I4/mmm$ space group have T_c's of 45 and 46 K [24]. The Na substitution might affect the magnetic order in phase-separated $K_xFe_{2-y}Se_2$ since the existence of a large magnetic moment in the antiferromagnetic phase was proposed to be important for the relatively high T_c's [40].

Due to the limited data points, it is difficult to unambiguously estimate $\mu_0 H_{c2}(0)$ for $H\perp c$. Based on results reported for similar Fe-based superconductors, $NdFeAsO_{0.7}F_{0.3}$ [7], $(Ba,K)Fe_2As_2$ [41], and $K_{0.8}Fe_{1.76}Se_2$ [9], $\mu_0 H_{c2}(0)$ shows a pronounced upward curvature for $H\|c$ while it tends to

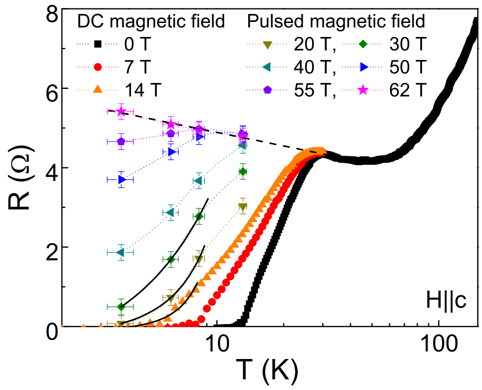

FIG. 4. (Color online) Temperature dependence of the resistance in several dc and pulsed magnetic fields for $H \| c$.

saturate for $H \perp c$. The real $\mu_0 H_{c2}(0)$ for $H \perp c$ might be smaller than we estimated. The calculated coherence lengths, using $\mu_0 H_{c2}^{\perp}(0) = \phi_0/2\pi\xi_{\perp}(0)\xi_{\|}(0)$ and $\mu_0 H_{c2}^{\|}(0) = \phi_0/2\pi\xi_{\perp}(0)^2$ based on the two-band BCS fit results, are similar to values obtained for as-grown and quenched $K_xFe_{2-y}Se_2$ and are shown in Table I [9,31].

Superconductivity in $K_{0.50(1)}Na_{0.24(4)}Fe_{1.52(3)}Se_2$ is completely suppressed above about 60 T for $H \| c$, allowing for a clear insight into the low-temperature electronic transport in the normal state (Fig. 4). Interestingly, we do not observe metallic transport below about 40 K, implying that a superconductor-to-insulator transition (SIT) is induced in high magnetic fields. Kondo-type magnetic scattering is not very likely since a field of 62 T should suppress spin-flip scattering [10]. A thermally activated semiconductorlike transport or variable range hopping (VRH) as occurring for Anderson localization is unlikely since the resistance in 62 T cannot be fit by $\ln R \propto -1/T$, $\ln R \propto T^{-\beta}$, with $\beta = 1/2$, 1/3, 1/4, and $\ln R \propto \ln T$ [42–44]. Instead, the resistance increases logarithmically with decreasing temperature in the normal state at 62 T, as shown with the dashed line in Fig. 4. Hence, the SIT might originate from the granular nature of $K_{0.50(1)}Na_{0.24(4)}Fe_{1.52(3)}Se_2$. In a bosonic SIT scenario, Cooper pairs are localized in granules [45,46]. When $H > H_{c2}$, virtual Cooper pairs form, yet they cannot hop to other granules when $T \to 0$, which induces the increase in resistivity as temperature decreases. The grain size can be estimated from $H_{c2}^0 \sim \phi_0/L\xi$, where L is the average grain radius and $\xi \approx 0.77$ nm is the average in-plane coherence length. The obtained $L = 62$ nm is in agreement with the phase-separation distance. The bosonic SIT mechanism in granular superconductors predicts $R = R_0 \exp(T/T_0)$ ("inverse Arrhenius law") in the superconducting region near the SIT when $H < H_{c2}$ due to the destruction of quasilocalized Cooper pairs by superconducting fluctuations. Our data in 14, 20, and 30 T might be fitted with this formula (solid lines in Fig. 4). We note that $R(H)$ near $\mu_0 H_{c2}(0)$ is nonmonotonic, similar as for granular Al and $La_{2-x}Sr_xCuO_4$ [10,46,47].

In summary, we reported the multiband nature of superconductivity in $K_{0.50}Na_{0.24}Fe_{1.52}Se_2$ as evidenced in the temperature dependence of the upper critical field and a SIT in high magnetic fields. Granular type-I but also copper-oxide superconductors are also intrinsically phase separated on the nanoscale [48–51]. Hence, a SIT in high magnetic fields seems to be connected with the intrinsic materials' granularity in inhomogeneous superconductors. This suggests that the insulating states found in cuprates as a function of magnetic field [10,11] or doping [52] might involve Josephson coupling of nanoscale grains as opposed to quasi-one-dimensional metallic stripes bridged by Mott-insulating regions in the spin-charge separated picture [53].

Work at Brookhaven is supported by the U.S. DOE under Contract No. DE-AC02-98CH10886 and in part by the Center for Emergent Superconductivity, an Energy Frontier Research Center funded by the U.S. DOE, Office for Basic Energy Science (C.P.). We acknowledge the support of the HLD at HZDR, member of the European Magnet Field Laboratory (EMFL). C.P. acknowledges support by the Alexander von Humboldt Foundation.

[1] Y. Kamihara, T. Watanabe, M. Hirano, and H. Hosono, J. Am. Chem. Soc. **130**, 3296 (2008).
[2] H. Lei, R. Hu, E. S. Choi, J. B. Warren, and C. Petrovic, Phys. Rev. B **81**, 094518 (2010).
[3] H. Lei, R. Hu, E. S. Choi, J. B. Warren, and C. Petrovic, Phys. Rev. B **81**, 184522 (2010).
[4] G. Fuchs, S. L. Drechsler, N. Kozlova, G. Behr, A. Kohler, J. Werner, K. Nenkov, C. Hess, R. Klingeler, J. E. Hamann-Borrero, A. Kondrat, M. Grobosch, A. Narduzzo, M. Knupfer, J. Freudenberger, B. Buchner, and L. Schultz, Phys. Rev. Lett. **101**, 237003 (2008).
[5] T. Kida, T. Matsunaga, M. Hagiwara, Y. Mizuguchi, Y. Takano, and K. Kindo, J. Phys. Soc. Jpn. **78**, 113701 (2009).
[6] F. Hunte, J. Jaroszynski, A. Gurevich, D. C. Larbalestier, R. Jin, A. S. Sefat, M. A. McGuire, B. C. Sales, D. K. Christen, and D. Mandrus, Nature (London) **453**, 903 (2008).
[7] J. Jaroszynski, F. Hunte, L. Balicas, Y. J. Jo, I. Raičević, A. Gurevich, D. C. Larbalestier, F. F. Balakirev, L. Fang, P. Cheng, Y. Jia, and H. H. Wen, Phys. Rev. B **78**, 174523 (2008).
[8] S. A. Baily, Y. Kohama, H. Hiramatsu, B. Maiorov, F. F. Balakirev, M. Hirano, and H. Hosono, Phys. Rev. Lett. **102**, 117004 (2009).
[9] E. D. Mun, M. M. Altarawneh, C. H. Mielke, V. S. Zapf, R. Hu, S. L. Bud'ko, and P. C. Canfield, Phys. Rev. B **83**, 100514(R) (2011).
[10] Y. Ando, G. S. Boebinger, A. Passner, T. Kimura, and K. Kishio, Phys. Rev. Lett. **75**, 4662 (1995).
[11] G. S. Boebinger, Y. Ando, A. Passner, T. Kimura, M. Okuya, J. Shimoyama, K. Kishio, K. Tamasaku, N. Ichikawa, and S. Uchida, Phys. Rev. Lett. **77**, 5417 (1996).

[12] S. Ono, Y. Ando, T. Murayama, F. F. Balakirev, J. B. Betts, and G. S. Boebinger, Phys. Rev. Lett. **85**, 638 (2000).
[13] H. Lei, M. Abeykoon, E. S. Bozin, K. Wang, J. B. Warren, and C. Petrovic, Phys. Rev. Lett. **107**, 137002 (2011).
[14] H. Lei and C. Petrovic, Phys. Rev. B **84**, 212502 (2011).
[15] H. Ryu, H. Lei, A. I. Frenkel, and C. Petrovic, Phys. Rev. B **85**, 224515 (2012).
[16] F. Han, H. Yang, B. Shen, Z.-Y. Wang, C. H. Li, and H. H. Wen, Philos. Mag. **92**, 2553 (2012).
[17] B. Hunter, International Union of Crystallography Commission on Powder Diffraction Newsletter No. 20 (Summer), 1998, p. 21, http://www.rietica.org
[18] N. Lazarevic, M. Abeykoon, P. W. Stephens, Hechang Lei, E. S. Bozin, C. Petrovic, and Z. V. Popovic, Phys. Rev. B **86**, 054503 (2012).
[19] D. H. Ryan, W. N. Rowan-Weetaluktuk, J. M. Cadogan, R. Hu, W. E. Straszheim, S. L. Budko, and P. C. Canfield, Phys. Rev. B **83**, 104526 (2011).
[20] Z. Wang, Y. J. Song, H. L. Shi, Z. W. Wang, Z. Chen, H. F. Tian, G. F. Chen, J. G. Guo, H. X. Yang, and J. Q. Li, Phys. Rev. B **83**, 140505 (2011).
[21] Y. Liu, Q. Xing, K. W. Dennis, R. W. McCallum, and T. A. Lograsso, Phys. Rev. B **86**, 144507 (2012).
[22] A. Ricci, N. Poccia, B. Josesph, G. Arrighetti, L. Barba, J. Plaiser, G. Campi, Y. Mizuguchi, H. Takeya, Y. Takano, N. L. Saini, and A. Bianconi, Supercond. Sci. Technol. **24**, 082002 (2011).
[23] W. Li, H. Ding, P. Deng, K. Chang, C. Song, K. He, L. Wang, X. Ma, J. P. Hu, X. Chen, and Q. K. Xue, Nat. Phys. **8**, 126 (2012).
[24] T. P. Ying, X. L. Chen, G. Wang, S. F. Jin, T. T. Zhou, X. F. Lai, H. Zhang, and W. Y. Wang, Sci. Rep. **2**, 426 (2012).
[25] J. Guo, S. Jin, G. Wang, S. Wang, K. Zhu, T. Zhou, M. He, and X. Chen, Phys. Rev. B **82**, 180520(R) (2010).
[26] M. Bendele, C. Marini, B. Joseph, G. M. Pierantozzi, A. S. Caporale, A. Bianconi, E. Pomjakushina, K. Conder, A. Krzton-Maziopa, T. Irifune, T. Shinmei, S. Pascarelli, P. Dore, N. L. Saini, and P. Postorino, Phys. Rev. B **88**, 180506 (2013).
[27] C. P. Bean, Phys. Rev. Lett. **8**, 250 (1962).
[28] E. M. Gyorgy, R. B. van Dover, K. A. Jackson, L. F. Schneemeyer, and J. V. Waszczak, Appl. Phys. Lett. **55**, 283 (1989).
[29] D. P. Shoemaker, D. Y. Chung, H. Claus, M. C. Francisco, S. Avci, A. Llobet, and M. G. Kanatzidis, Phys. Rev. B **86**, 184511 (2012).
[30] M. Yi, D. H. Lu, R. Yu, S. C. Riggs, J.-H. Chu, B. Lv, Z. K. Liu, M. Lu, Y.-T. Cui, M. Hashimoto, S.-K. Mo, Z. Hussain, C. W. Chu, I. R. Fisher, Q. Si, and Z.-X. Shen, Phys. Rev. Lett. **110**, 067003 (2013).
[31] H. Lei and C. Petrovic, Europhys. Lett. **95**, 57006 (2011).
[32] N. R. Werthamer, E. Helfand, and P. C. Hohenberg, Phys. Rev. **147**, 295 (1966).
[33] T. P. Orlando, E. J. McNiff, Jr., S. Foner, and M. R. Beasley, Phys. Rev. B **19**, 4545 (1979).
[34] P. B. Allen, in *Handbook of Superconductivity*, edited by C. P. Poole, Jr. (Academic, New York, 1999), p. 478.
[35] A. Gurevich, Phys. Rev. B **67**, 184515 (2003).
[36] H. Lei, D. Graf, R. Hu, H. Ryu, E. S. Choi, S. W. Tozer, and C. Petrovic, Phys. Rev. B **85**, 094515 (2012).
[37] V. A. Gasparov, A. Audouard, L. Drigo, A. I. Rodigin, C. T. Lin, W. P. Liu, M. Zhang, A. F. Wang, X. H. Chen, H. S. Jeevan, J. Maiwald, and P. Gegenwart, Phys. Rev. B **87**, 094508 (2013).
[38] A. Kreisel, Y. Wang, T. A. Maier, P. J. Hirschfeld, and D. J. Scalapino, Phys. Rev. B **88**, 094522 (2013).
[39] X.-W. Yan and M. Gao, J. Phys.: Condens. Matter **24**, 455702 (2012).
[40] S.-M. Huang, Ch.-Y. Mou, and T.-K. Lee, Phys. Rev. B **88**, 174510 (2013).
[41] H. Q. Yuan, J. Singleton, F. F. Balakirev, S. A. Baily, G. F. Chen, J. L. Luo, and N. L. Wang, Nature (London) **457**, 565 (2009).
[42] N. F. Mott, Philos. Mag. **19**, 835 (1969).
[43] E. Abrahams, P. W. Anderson, D. C. Licciardello, and T. V. Ramakrishnan, Phys. Rev. Lett. **42**, 673 (1979).
[44] L. P. Gor'kov, A. I. Larkin, and D. E. Khmel'nitskii, JETP Lett. **30**, 228 (1979).
[45] V. F. Gantmakher and V. T. Dolgopolov, Phys. Usp. **53**, 1 (2010).
[46] I. S. Beloborodov, A. V. Lopatin, V. M. Vinokur, and K. B. Efetov, Rev. Mod. Phys. **79**, 469 (2007).
[47] A. Gerber, A. Milner, G. Deutscher, M. Karpovsky, and A. Gladkikh, Phys. Rev. Lett. **78**, 4277 (1997).
[48] M. Strongin, R. S. Thompson, O. F. Kammerer, and J. E. Crow, Phys. Rev. B **1**, 1078 (1970).
[49] Y. Imry and M. Strongin, Phys. Rev. B **24**, 6353 (1981).
[50] K. M. Lang, V. Madhavan, J. E. Hoffman, H. Eisaki, S. Uchida, and J. C. Davis, Nature (London) **415**, 412 (2002).
[51] I. Zeljkovic, Z. Xu, J. Wen, G. Gu, R. Markiewitz, and J. E. Hoffman, Science **337**, 320 (2012).
[52] Y. Fukuzumi, K. Mizuhashi, K. Takenaka, and S. Uchida, Phys. Rev. Lett. **76**, 684 (1996).
[53] V. J. Emery, S. A. Kivelson, and O. Zachar, Phys. Rev. B **56**, 6120 (1997).